WATER RESOURCES RESEARCH, VOL. 29, NO. 8, PAGES 2533–2544, AUGUST 1993

A Multicomponent Decomposition of Spatial Rainfall Fields 2. Self-Similarity in Fluctuations

PRAVEEN KUMAR[1] AND EFI FOUFOULA-GEORGIOU

St. Anthony Falls Hydraulic Laboratory, Department of Civil and Mineral Engineering, University of Minnesota, Minneapolis

In the first paper (Kumar and Foufoula-Georgiou, this issue) we developed a methodology for the segregation of large- and small-scale features (fluctuations) of spatial rainfall fields. In this paper we develop a framework for testing the presence and studying the nature of self-similarity in the fluctuations. It is found that rainfall fluctuations may be approximated by stable distributions and show scaling up to a certain scale. We define and estimate parameters that characterize the scaling and spatial dependence of the rainfall fluctuations and we use these parameters, estimated for several radar rainfall frames (in time), to relate to and identify the evolutionary nature of rainfall. Two radar depicted rainfall fields have been extensively analyzed: a severe spring time midlatitude squall line storm and a mild midlatitude winter type storm. The type of scaling in rainfall fluctuations shows significant variation from one rainfall field to another.

1. INTRODUCTION

In the work by *Kumar and Foufoula-Georgiou* [this issue] the hypothesis was set forward that rainfall can be decomposed into a large-scale component representing the mean behavior of the process and small-scale fluctuations which exhibit self-similarity. In that paper we developed a methodology for segregating large- and small-scale features. The basic requirements from any methodology designed for this purpose are (1) data windowing capability so that nonhomogeneities can be localized, (2) adjustable window size so that no a priori information on the size of these features is required, and (3) consistency across scales, i.e., features extracted at a certain scale directly from the data, or through an intermediate scale, should be the same. The methodology (based on orthogonal wavelets) developed in the first paper [see *Kumar and Foufoula-Georgiou*, this issue] elegantly embodies these requirements. The multiscale segregation achieved is such that statistics like the mean and correlation function of the component processes are additive. Also, the orthogonality of scale function and wavelets provide some additional optimality properties of multiscale discretization of the process or its fluctuations, without any redundancy or loss of information [*Kumar and Foufoula-Georgiou*, this issue, section 4]. These properties are particularly attractive for the statistical analysis and inference of the rainfall process.

By applying the above methodology we accomplished a decomposition of the inner variability field $X(t)$, i.e., the rainfall field conditioned on being positive, into two uncorrelated components

$$X(\mathbf{t}) = \bar{X}(\mathbf{t}) + X'(\mathbf{t}) \tag{1}$$

where the mean process $\bar{X}(\mathbf{t})$ and fluctuation process $X'(\mathbf{t})$ were approximated using scale functions Φ and wavelets Ψ^i, respectively, as $\bar{X}(\mathbf{t}) \approx \bar{X}_{m_0}(\mathbf{t})$ and $X'(\mathbf{t}) = X'_1(\mathbf{t}) + X'_2(\mathbf{t}) + X'_3(\mathbf{t})$ where

$$\bar{X}_{m_0}(\mathbf{t}) = \sum_{n,k} (X, \Phi_{m_0 nk})\Phi_{m_0 nk}(\mathbf{t}) \tag{2}$$

$$X'_i(\mathbf{t}) = \sum_{m \geq m_0} \sum_{n,k} (X, \Psi^i_{mnk})\Psi^i_{mnk}(\mathbf{t}). \tag{3}$$

where m_0 is the critical scale that segregates large- and small-scale behavior. We showed that these components are physically meaningful. $\bar{X}(\mathbf{t})$ represents the large-scale behavior of the process and $X'_1(\mathbf{t})$, $X'_2(\mathbf{t})$, and $X'_3(\mathbf{t})$ capture the horizontal, vertical, and diagonal high correlations of the fluctuation process.

In this paper we hypothesize that $X'(\mathbf{t})$ may exhibit scaling (in the sense defined below), and we test this hypothesis. We say that the fluctuation process $X'(\mathbf{t})$ scales if

$$\{X'_1(\lambda \mathbf{t})\} \overset{d}{=} \{\lambda^{H_1} X'_1(\mathbf{t})\}, \tag{4}$$

$$\{X'_2(\lambda \mathbf{t})\} \overset{d}{=} \{\lambda^{H_2} X'_2(\mathbf{t})\}, \tag{5}$$

$$\{X'_3(\lambda \mathbf{t})\} \overset{d}{=} \{\lambda^{H_3} X'_3(\mathbf{t})\}. \tag{6}$$

where the above equalities are in terms of the joint distribution of the corresponding fluctuation processes. The scaling exponents H_1, H_2, and H_3 need not be the same. In the event that the process is "isotropically self-similar," the three scaling exponents H_1, H_2, and H_3 are equal. The difference in the values of H_1, H_2, and H_3 help us characterize differences in the dependence structure of the storm in the three directions.

In general, the fluctuations may have finite or infinite variance and be dependent or independent. A general framework for the identification of self-similarity and parameter estimation techniques for a class of distributions for which self-similarity holds are developed in section 2. The method described here is geared toward fitting distributions to the fluctuations and not just performing moment analysis as in the work by *Gupta and Waymire* [1990]. This overcomes both drawbacks of moment analysis, i.e., unreliability of higher-order moments and taking moments when moments

[1]Now at Hydrologic Sciences Branch, Laboratory for Hydrospheric Processes, NASA Goddard Space Flight Center, Greenbelt, Maryland.

Paper number 93WR00549.
0043-1397/93/93WR-00549$05.00

of the distribution under examination might not exist. As is discussed by *Kumar and Foufoula-Georgiou* [this issue] radar rainfall intensities should be interpreted as integral quantities over the measuring space-time interval instead of point values. The theory of self-similarity needs to be extended to include such generalized processes. This is developed in section 3.

In general, when the wavelet coefficients have a distribution with infinite variance then the process is no longer square integrable, i.e., L^2. Some of the nuances introduced by this situation in the application of the multiresolution framework are discussed in section 4. In section 5 we present the analysis of two storms, a severe midlatitude squall line storm and a midlatitude winter type storm. It is found that scaling models can provide reasonable representations of rainfall fluctuations up to a certain scale and the type of scaling varies significantly from one storm type to another. Some closing remarks are made in section 6.

2. Self-Similar Probability Distributions

2.1. *Definition*

The distinguishing feature of self-similar processes is their inherent lack of dependence on the scale of description of the process. Mathematically, such processes are defined as processes whose finite dimensional joint distribution function satisfies equation [see *Lamperti*, 1962]

$$Pr\ (\lambda^{-H}X(\lambda t_1) < x_1, \cdots, \lambda^{-H}X(\lambda t_n) < x_n) = Pr\ (X(t_1) < x_1, \cdots, X(t_n) < x_n). \quad (7)$$

which is also written as

$$\{X(\lambda t)\} \overset{d}{=} \{\lambda^H X(t)\} \qquad H \in \mathbf{R},\ \lambda \in \mathbf{R}^+ \quad (8)$$

By nature of the transformation involved, the n dimensional multivariate joint probability distribution function, $p(\mathbf{x};\ \mathbf{t})$, $\mathbf{x},\ \mathbf{t} \in \mathbf{R}^n$, of the random vector $\mathbf{X} = \{X(t_1), \cdots, X(t_n)\}$, necessarily satisfies

$$p(\mathbf{x};\ \mathbf{t}) = \lambda^H p(\lambda^H \mathbf{x};\ \lambda \mathbf{t}) \quad (9)$$

The marginal distribution function satisfies

$$p(x;\ t) = \lambda^H p(\lambda^H x;\ \lambda t). \quad (10)$$

The notation $p(\mathbf{x};\ \mathbf{t})$ indicates that the distribution function of $\mathbf{X}$ is specified by parameters that depend on $\mathbf{t}$. The above condition (9) can be translated into a requirement for the characteristic function of the multidimensional distribution, $\rho(\boldsymbol{\xi};\ \mathbf{t})$, as

$$\rho(\boldsymbol{\xi};\mathbf{t}) = \int p(\mathbf{x};\mathbf{t}) e^{-i\boldsymbol{\xi}\cdot\mathbf{x}}\, d\mathbf{x} = \lambda^H \int p(\lambda^H \mathbf{x};\lambda\mathbf{t}) e^{-i\boldsymbol{\xi}\cdot\mathbf{x}}\, d\mathbf{x}$$

which on substituting $\lambda^H \mathbf{x} = \mathbf{y}$ gives

$$\rho(\boldsymbol{\xi};\ \mathbf{t}) = \rho(\lambda^{-H}\boldsymbol{\xi};\ \lambda\mathbf{t}) \quad (11)$$

or, equivalently, for the characteristic function of the marginal distribution

$$\rho(\xi;\ t) = \rho(\lambda^{-H}\xi;\ \lambda t). \quad (12)$$

Relationships between moments (if they exist) of the marginal distribution can be obtained as

$$E[X^h(t)] = \int x^h p(x;\ t)\, dx = \int x^h \lambda^H p(\lambda^H x;\ \lambda t)\, dx$$

which on substitution of $\lambda^H x = y$ gives

$$E[X^h(t)] = \lambda^{-hH} E[X^h(\lambda t)] \quad (13)$$

It is noted that if the distribution is symmetric about the origin then all the odd moments are zero for which the above equation holds trivially.

In general, the probability distribution $p(\mathbf{x};\ \mathbf{t})$ satisfying (9) can be classified into one of the three categories: (1) Gaussian, (2) non-Gaussian infinite variance distribution (stable distributions), and (3) non-Gaussian finite variance distributions. The authors are not aware of any known examples in the third category and hence this category will not be discussed further. Below we elaborate on the first two categories which will be used in the analysis of rainfall fluctuations.

2.2. *Gaussian Distributions*

In general, the finite dimensional Gaussian distribution is given by

$$p(\mathbf{x};\ \mathbf{t}) = \frac{1}{(2\pi|\Sigma(\mathbf{t})|)^{1/2}} \cdot \exp\{-\tfrac{1}{2}([\mathbf{x} - \boldsymbol{\mu}(\mathbf{t})] \cdot \Sigma^{-1}(\mathbf{t})[\mathbf{x} - \boldsymbol{\mu}(\mathbf{t})])\} \quad (14)$$

where $\Sigma(\mathbf{t})$ is the covariance matrix, $\boldsymbol{\mu}(\mathbf{t}) \in \mathbf{R}^n$ is the mean vector, and $\mathbf{x} \cdot \mathbf{y}$ represents the inner product of two vectors. Let us assume that, in accordance with (13),

$$\boldsymbol{\mu}(\lambda\mathbf{t}) = \lambda^H \boldsymbol{\mu}(\mathbf{t}) \qquad \Sigma(\lambda\mathbf{t}) = \lambda^{2H}\Sigma(\mathbf{t}) \quad (15)$$

implying $\Sigma^{-1}(\lambda\mathbf{t}) = \lambda^{-2H}\Sigma^{-1}(\mathbf{t})$. It can then be verified that under these conditions, and only under these conditions, $p(\mathbf{x};\ \mathbf{t})$ satisfies (9).

2.3. *Stable Distributions*

2.3.1. *Definition and properties.* As is described by *Feller* [1971, p. 169], if X, X_1, X_2, $\cdots$ are mutually independent random variables with a common distribution F_S, then the (nondegenerate) distribution F_S is said to be stable if for each $n \in \mathbf{Z}$, there exist constants $C_n > 0$ and r_n such that

$$S_n \overset{d}{=} C_n X + r_n \quad (16)$$

where $S_n = X_1 + X_2 + \cdots + X_n$. The norming constant C_n is of the form $n^{1/\alpha}$ with $0 < \alpha \leq 2$. The constant α is called the characteristic exponent of the distribution F_S. The distribution F_S is termed strictly stable if $r_n = 0$. Thus by the defining property (16) stable distributions are invariant under convolution up to a scale and location parameter.

Closed-form expressions for the probability density functions (pdf) of stable densities exist only for a few selected values of α. In general, the stable densities are described through their characteristic function which is given by [see *Stuart and Ord*, 1987, p. 147]

$$\rho(\xi) = \exp\{i\mu\xi - |c\xi|^{\alpha}[1 + i\beta\ \text{sgn}\ (\xi)w(|\xi|, \alpha)]\} \quad (17)$$

where

$$w(|\xi|, \alpha) = \tan\left(\frac{\pi\alpha}{2}\right) \qquad \alpha \neq 1, \quad (18)$$

$$w(|\xi|, \alpha) = \left(\frac{2}{\pi}\right)\log|\xi| \qquad \alpha = 1$$

$$\text{sgn}\ (\xi) = 1 \qquad \xi > 0$$

$$\text{sgn}\ (\xi) = 0 \qquad \xi = 0 \quad (19)$$

$$\text{sgn}\ (\xi) = -1 \qquad \xi < 0$$

and $-\infty < \mu < \infty$, $c > 0$, $0 < \alpha \leq 2$, and $-1 \leq \beta \leq 1$. Here μ is a location parameter, c is a scale parameter, and β a skewness parameter.

For $\alpha = 2$, $\rho(\xi)$ gives the characteristic function of the normal density with mean μ and variance $2c^2$. For $\alpha = 1$ and $\beta = 0$ we get the Cauchy distribution with pdf $(1/\pi)\{c/[c^2 + (x - \mu)^2]\}$. For $\alpha = 1/2$ and $\beta = -1$ we get a pdf given by

$$p(x) = \frac{1}{(2\pi)^{1/2}}x^{-3/2}e^{-1/2x} \qquad x > 0$$

$$p(x) = 0 \qquad x \leq 0$$

Although, closed-form expressions do not exist for other values of (α, β), the probability densities can be numerically obtained through certain series expansions [see *Holt and Crow*, 1973].

A multidimensional extension of the characteristic function (17) for symmetric stable distributions is given by [see *Press*, 1982, equation (6.5.9)]

$$\rho_{\mathbf{X}}(\boldsymbol{\xi}) = \exp\{i\boldsymbol{\mu}\cdot\boldsymbol{\xi} - \tfrac{1}{2}(\boldsymbol{\xi}\cdot\Omega\boldsymbol{\xi})^{\alpha/2}\} \quad (20)$$

where Ω is a positive semidefinite $n \times n$ matrix called scale matrix and $\mathbf{X}$, $\boldsymbol{\xi}$, $\boldsymbol{\mu} \in \mathbf{R}^n$. It is remarked that the joint distribution function (20) does not characterize all possible multidimensional symmetric distributions [see *Paulauskas*, 1976].

Stable distributions possess the following interesting properties which will be used in setting up the framework of analysis of rainfall fluctuations.

1. The characteristic function of the standardized variable $(X - \mu)/c$ is of the form given in (17) with $\mu = 0$, $c = 1$; equivalently,

$$F_S(x; \alpha, \beta, \mu, c) = F_S\left(\frac{x - \mu}{c}; \alpha, \beta, 0, 1\right). \quad (21)$$

2. The pdf of stable densities satisfy $p(-x; \alpha, \beta) = p(x; \alpha, -\beta)$.

3. The pdfs of stable densities are unimodal [see *Gawronski*, 1984] and are symmetrical if $\beta = 0$. They have thick tails of the form $P(X > x) \sim C_1x^{-\alpha}$ and $P(X < -x) \sim C_2x^{-\alpha}$ as $x \to \infty$, $C_1, C_2 \in \mathbf{R}^+$, where $\sim$ indicates an asymptotic equality with increasing x. Evidently, the thickness of the tail increases as α decreases and results in the following property.

4. If the random variable X has a stable distribution then $E[|X|^h]$ exists only for $h < \alpha$, $0 < \alpha < 2$. The mean exists for $1 < \alpha \leq 2$, but for $0 < \alpha \leq 1$ neither mean nor variance exists. Thus normal distributions are the only stable distributions with finite variance. It is noted that moments of all orders of the logarithm of absolute values of stable random variables, i.e., $\log|X|$, exist [see *Zolotarev*, 1986, p. 213].

2.3.2. *Self-similar stable distributions.* Not all stable distributions, i.e., distributions characterized by (20), satisfy the condition (11) of self-similarity. For rainfall analysis we focus on symmetric stable distributions which are self-similar, although more general forms are possible. We consider stable distributions whose joint characteristic function can be written as

$$\rho(\boldsymbol{\xi}; \mathbf{t}) = \exp\{i\boldsymbol{\mu}(\mathbf{t})\cdot\boldsymbol{\xi} - \tfrac{1}{2}(\boldsymbol{\xi}\cdot\Omega(\mathbf{t})\boldsymbol{\xi})^{\alpha/2}\} \quad (22)$$

where the matrix $\Omega(\mathbf{t})$ is positive semidefinite. Let us assume that $\Omega(\mathbf{t})$ is such that $\Omega(\lambda\mathbf{t}) = \lambda^{2H}\Omega(\mathbf{t})$. In order that $\rho(\boldsymbol{\xi}; \mathbf{t}) = \rho(\lambda^{-H}\boldsymbol{\xi}; \lambda\mathbf{t})$, we in addition need to have $\boldsymbol{\mu}(\lambda\mathbf{t}) = \lambda^H\boldsymbol{\mu}(\mathbf{t})$. In the event that $\boldsymbol{\mu}(\mathbf{t}) = 0$, the condition $\Omega(\lambda\mathbf{t}) = \lambda^{2H}\Omega(\mathbf{t})$ is sufficient for $\rho(\boldsymbol{\xi}; \mathbf{t})$ to be the characteristic function of a self-similar distribution. In general, the marginal characteristic function of a symmetric stable distribution ($\beta = 0$) with $\mu = 0$ is given by

$$\varrho(\xi; t) \equiv \rho(\xi; t)|_{\mu=\beta=0} = \exp(-|c(t)\xi|^{\alpha}). \quad (23)$$

For it to be self-similar, i.e., satisfy (11), we need to have

$$c(\lambda t) = \lambda^H c(t) \quad (24)$$

or, equivalently,

$$\log c(\lambda t) = H\log\lambda + \log c(t). \quad (25)$$

A typical example of such a process whose joint characteristic function satisfies (22) and the scale parameter $c(t)$ of the marginal characteristic function satisfies (25) is constructed in the Appendix. This process (which is a particular construction of a fractional Levy motion process) can be used to model the multidimensional structure of rainfall fluctuations, since, as will be seen from the rainfall data analysis, rainfall fluctuations exhibit long-range dependence with probability distributions having infinite variance.

2.3.3. *Parameter estimation.* Parameter estimation for stable distributions is tricky because (1) moments do not exist and therefore method of moments cannot be used and (2) pdfs cannot be written in an explicit form, and hence method of maximum likelihood cannot be used. Here we consider the parameter estimation of a class of univariate stable distributions that are symmetric ($\beta = 0$) and have finite mean, i.e., $1 < \alpha \leq 2$. For this case the parameters can be obtained as described here which is a slight modification of the method discussed by *Arad* [1980]. For $1 < \alpha \leq 2$, the location parameter μ equals the mean which can be seen from $(1/i)(d/d\xi)\rho(0) = \mu$. Hence the sample mean can be used as an estimator for μ. Subtracting the mean μ we get a symmetric stable distribution whose characteristic function is given by

$$\varrho(\xi) = \exp(-|c\xi|^{\alpha}). \quad (26)$$

Therefore $\log\varrho(\xi) = -|c\xi|^{\alpha} = -\gamma|\xi|^{\alpha}$, where $\gamma = c^{\alpha}$. Equivalently,

$$\log(-\log\varrho(\xi)) = \alpha(\log c + \log|\xi|) = \alpha\log|\xi| + \log\gamma. \quad (27)$$

The sample characteristic function is estimated as

$$\hat{\varrho}(\xi) = \frac{1}{n}\sum_{j=1}^{n} \exp(iX_j\xi)$$

$$= \frac{1}{n}\sum_{j=1}^{n} \cos(X_j\xi) + \frac{i}{n}\sum_{j=1}^{n} \sin(X_j\xi)$$

$$\equiv C(\xi) + iS(\xi) \tag{28}$$

Notice that since $|\exp(iX_j\xi)|$ is always bounded by unity, $\hat{\varrho}(\xi)$ always exists. Comparing (27) and (28) we see that the parameters α and $\log \gamma$ can be obtained as slopes and intercepts of the linear regression on $\log(-\log C(\xi))$. Considering the periodic nature of the cosine function, one needs to consider several values of ξ only between $0 < \xi \leq \pi/2$ for the regression. For rainfall analysis we use the method described above as it is found that $1 < \alpha \leq 2$. For the case $0 < \alpha \leq 1$, if μ can be obtained by some other means, say, by the estimation of the location of the mode, then the above estimation procedure can be used for this range of α also. For parameter estimation in the general case see *Press* [1982].

3. Generalized Self-Similar Processes

We would like to extend the class of self-similar processes so as to also include processes that do not have point values and are meaningful only when defined through an integral transform, $X_\varphi(t) = \int X(u)\varphi(t-u)\,du$, such as the rainfall process. Toward this objective we use the definition of *Dobrushin* [1978]. We shall call a process $X_\varphi(t)$ self-similar if

$$\left\{\int X(t)\,\frac{1}{\lambda}\,\varphi\left(\frac{t-u}{\lambda}\right)dt\right\} \overset{d}{=} \left\{\lambda^H \int X(t)\varphi(t-u)\,dt\right\} \tag{29}$$

which is the analogue of equation $\{X(\lambda t)\} \overset{d}{=} \{\lambda^H X(t)\}$. For processes that are self-similar in the sense of (8), the above relationship holds. If $\varphi(t)$ has N vanishing moments, i.e.,

$$\int t^k\varphi(t)\,dt = 0 \qquad k = 0, \cdots, N-1 \tag{30}$$

and $X_\varphi(t)$ is stationary and self-similar in the sense of (29), then we say that the process is self-similar with (generalized) stationary increments of order N. As is discussed by *Kumar and Foufoula-Georgiou* [this issue], wavelets with N vanishing moments provide a very attractive tool for studying such processes.

In the event that we have a process on a d dimensional space, i.e., $X(\mathbf{t})$ such that $\mathbf{t} \in \mathbf{R}^d$, then the equivalent scaling equation is

$$\left\{\int X(\mathbf{t})\,\frac{1}{\lambda^d}\,\varphi\left(\frac{\mathbf{t}-\mathbf{u}}{\lambda}\right)d\mathbf{t}\right\} \overset{d}{=} \left\{\lambda^H \int X(\mathbf{t})\varphi(\mathbf{t}-\mathbf{u})\,d\mathbf{t}\right\}, \qquad \mathbf{t}, \mathbf{u} \in \mathbf{R}^d \tag{31}$$

and the finite dimensional multivariate distribution function satisfies

$$p(\mathbf{x};\mathbf{t}) = \lambda^H p(\lambda^H\mathbf{x};\lambda\mathbf{t}) \tag{32}$$

where $\mathbf{x}$ is now a value assumed by the random variable $X_\varphi(\mathbf{t})$ and $\mathbf{t}$ is a ν dimensional vector whose elements are d dimensional vectors $\mathbf{t} \in \mathbf{R}^d$. Equivalently, the characteristic function satisfies

$$\rho(\xi;\mathbf{t}) = \rho(\lambda^{-H}\xi;\lambda\mathbf{t}). \tag{33}$$

The probability distribution (32) of the random variables $X_\varphi(\mathbf{t}-\mathbf{u})$ could lie in either of the three classes discussed earlier, i.e., generalized Gaussian or stable or non-Gaussian finite variance distribution. When $d = 2$, we will call $X(\mathbf{t})$, satisfying (31), self-similar generalized random field. It is in this framework that we will study self-similarity of fluctuations obtained using wavelet transform of the inner variability rainfall field $X(\mathbf{t})$.

Now a few words of clarification.

1. For multidimensional processes, i.e., processes on d dimensional space $\mathbf{R}^d$, the requirements of self-similarity developed on the distribution function (equation (9)) or the characteristic function (equation (11)) for one-dimensional self-similar processes do not change. Only the way in which the parameters of the distribution (or characteristic) function depend on the dimension of the underlying space being considered changes. For instance, for generalized Gaussian self-similar processes, condition (15) changes to

$$\boldsymbol{\mu}(\lambda\mathbf{t}) = \lambda^H\boldsymbol{\mu}(\mathbf{t}), \qquad \Sigma(\lambda\mathbf{t}) = \lambda^{2H}\Sigma(\mathbf{t}) \tag{34}$$

where $\mathbf{t} \in \mathbf{R}^\nu$ is a ν dimensional vector whose elements are two-dimensional vectors $\mathbf{t} \in \mathbf{R}^2$, and likewise for other distributions.

2. If $\int \varphi(\mathbf{t})\,d\mathbf{t} = 1$, $\mathbf{t} \in \mathbf{R}^d$, i.e., $\varphi(\mathbf{t})$ is an averaging kernel, then $\int (1/\lambda^d)\varphi[(\mathbf{t}-\mathbf{u})/\lambda]\,d\mathbf{t} = 1$, which illustrates the reason for using the prefactor $1/\lambda^d$ in the left-hand side of (31). Due to this, the dimension d of the underlying space does not appear along with the scaling exponent H in the (31) and (33).

3. For the multidimensional case, the condition (30) can be written as

$$\int \mathbf{t}^k\varphi(\mathbf{t})\,d\mathbf{t} = 0 \qquad k = 0, \cdots, N-1 \tag{35}$$

where $\mathbf{t}^k = t_1^{k_1}\cdots t_d^{k_d}$ and $k_1 + \cdots + k_d = k$ for the d dimensional vector $\mathbf{t} = [t_1 \cdots t_d]$.

4. Stable Fluctuations

The mathematical representation of the rainfall component processes $X'_1(\mathbf{t})$, $X'_2(\mathbf{t})$, and $X'_3(\mathbf{t})$ becomes involved if their discretizations (X, Ψ^i_{mnk}) are found to have a stable distribution. In this event the fluctuation processes $X'_1(\mathbf{t})$, $X'_2(\mathbf{t})$, and $X'_3(\mathbf{t})$ do not belong to the Hilbert space $L^2(\mathbf{R})$. If $1 < \alpha < 2$ then these processes belong to L^P spaces where $P = \alpha$. However, the entire wavelet transform framework described by *Kumar and Foufoula-Georgiou* [this issue] for L^2 is valid for $L^P(1 < P < \infty)$ as wavelets constitute unconditional bases for these spaces [see *Daubechies*, 1992, theorem 9.1.6]. Properties *P*1, *P*2, and *P*3 [see *Kumar and Foufoula-Georgiou*, this issue, section 4] which do not

require orthogonality but merely linear independence, ensure that $\{(X, \Psi^i_{mnk})\}_{i=1,3}$ and $\{(X, \Phi_{mnk})\}$ may be regarded as optimal discretizations of the fluctuation and the average processes, respectively, for our purpose of stochastic identification and representation. The case of $0 < \alpha \leq 1$ is more complicated and will not be considered here.

In studying the fluctuation process two cases may arise, i.e., the distribution functions of the fields X'_{d1}, X'_{d2}, and X'_{d3} (which are the discretizations of the fields $X'_1(\mathbf{t})$, $X'_2(\mathbf{t})$, and $X'_3(\mathbf{t})$, respectively) may have (1) different characteristic exponents α_1, α_2, and α_3, respectively, or (2) the same characteristic exponent. If the fluctuation components $\{X'_{di}\}_{i=1,2,3}$ have different scaling exponents then they are described by different distribution functions. Hence they can be analyzed independently of each other for scaling characteristics. If the rainfall fluctuation components have the same characteristic exponent α, then a weaker condition of being "uncorrelated" in a sense to be discussed below is sufficient to justify the independent analysis of these components.

Recall from (22) that the symmetric joint stable distribution of two random variables $X_1 = X'_{di}(\mathbf{t}_1)$ and $X_2 = X'_{dj}(\mathbf{t}_2)$ $\{i, j \in [1, 3], i \neq j\}$, $\mathbf{t}_1, \mathbf{t}_2 \in \mathbf{R}^2$, obtained from two different components of the fluctuations is given as

$$\rho_{X_1,X_2}(\xi_1, \xi_2) = \exp\left\{-\frac{1}{2}\left((\xi_1 \ \xi_2)\begin{pmatrix}\Omega_{11} & \Omega_{12}\\ \Omega_{21} & \Omega_{22}\end{pmatrix}\begin{pmatrix}\xi_1\\ \xi_2\end{pmatrix}\right)^{\alpha/2}\right\}. \tag{36}$$

where Ω is a positive definite matrix. We define an association parameter

$$\gamma = \frac{\Omega_{12}}{(\Omega_{11}\Omega_{22})^{1/2}}. \tag{37}$$

In the event that $\alpha = 2$ (Gaussian distribution) γ gives the correlation coefficient of X_1 and X_2. In general, the following properties hold for γ [see *Press*, 1972]: (1) $-1 \leq \gamma \leq 1$; (2) if X_1 and X_2 are stochastically independent then $\gamma = 0$; and (3) if $\gamma = 1$ then the distribution is degenerate. Thus γ possesses all the properties of correlation coefficient. The condition we require for the independent analysis of the rainfall fluctuation components is that $\gamma = 0$ $\forall i, j$. For the purpose of this research we will assume that this condition holds without formally proving it. We will call random variables satisfying this condition uncorrelated (although it is reminded that these random variables do not have second or higher order moments) and rely on the context to clarify the sense in which this term is used.

5. Data Analysis

5.1. *Analysis Framework*

To find if the fluctuations of the rainfall process scale in the sense of (4)–(6) we study the marginal distribution function of the discretizations of the component processes $\{X'_{di,m}\}_{i=1,2,3}$ at different scales 2^{-m}. The steps involved in the analysis are summarized below.

1. Check if the discretization of rainfall fluctuations $X'_{di,m}$ at each resolution obeys a stable law or can be approximated by one. At each resolution m, the characteristic exponent α and the scale parameter c is estimated by the method described in section 2.3.3. The Gaussian case is treated as a special case for $\alpha = 2$ with variance $\sigma^2 = 2c^2$.

2. Check the goodness of fit. Having estimated the parameters by the above procedure, the theoretical and empirical cumulative distribution function (CDF) is plotted for each component at each scale to see the goodness of fit. The empirical CDF was obtained using Weibull plotting positions [*Haan*, 1977]. The theoretical CDFs for various α and c were estimated by the following procedure. (1) Probability distribution function $p_S(x)$ for a range of values of x were numerically obtained for the values of $\alpha = \{1, 1.1, 1.2, 1.25, 1.3, 1.375, 1.4, 1.5, 1.5556, 1.6, 1.625, 1.6667, 1.7, 1.75, 1.7778, 1.8, 1.875, 1.9, 2.0\}$ at $c = 1$ using the procedure described by *Holt and Crow* [1973] (also see section 2.3.1). The results matched exactly with those given by *Holt and Crow* [1973]. (2) The pdf thus obtained were numerically integrated to get CDFs at the respective values of α and $c = 1$. (3) For all other values of α the CDF was obtained by linear interpolation. (4) CDFs for $c \neq 1$ were obtained using the relation (see equation (21))

$$F_s(x;\ \alpha,\ \beta = 0,\ \mu = 0,\ c) = F_s\left(\frac{x}{c};\ \alpha,\ \beta = 0,\ \mu = 0,\ c = 1\right).$$

3. If the rainfall fluctuations can be described by a stable law, test to see if they exhibit scaling. This test is based on the fact that if a component is scaling, the scale coefficient c estimated at different scales λ will show log-log linearity with λ (see equation (25)).

4. If the rainfall fluctuations are not self-similar for all scales, determine the critical resolution m_0 up to which scaling is observed and estimate H. The resolution m_0 is determined from the point of departure from linearity in the log-log plot of scaling parameter c with scale λ. The slope of the graph up to scale 2^{-m_0} gives the estimate of the parameter H.

5. Study the evolutionary behavior of the storm by studying the changes in $\{\alpha_i\}_{i=1,2,3}$ and $\{H_i\}_{i=1,2,3}$ across frames. Under our hypothesis the characteristic exponent $\{\alpha_i\}$ for the marginal distribution of $\{X'_{di,m}\}_{i=1,2,3}$ is expected to be the same for all resolutions m. However, variations were observed in the estimated values of α. The variations differed between various data sets but in general it was observed that variations were larger for smaller α. We took the mean $\bar{\alpha}_i$, obtained over various scales 2^{-m} up to the critical scale 2^{-m_0}, as the representative value of α_i for that frame. To study the evolutionary structure of the storm, $\bar{\alpha}_i$ and H_i were plotted for various frames for all data sets.

5.2. *Results*

The fluctuations of two rainfall fields, one squall line storm and a convective winter type storm, were analyzed using the above framework for the purpose of identifying the type of scaling present and estimating the scaling parameters. The squall line storm data set was described by *Kumar and Foufoula-Georgiou* [this issue]. The winter type storm was monitored by the same radar on February 22, 1985, over Norman, Oklahoma. Rainfall intensities for the squall line storm are available at two temporal integration scales, 1 hour and 10 min, for 360 azimuths, with every azimuth containing

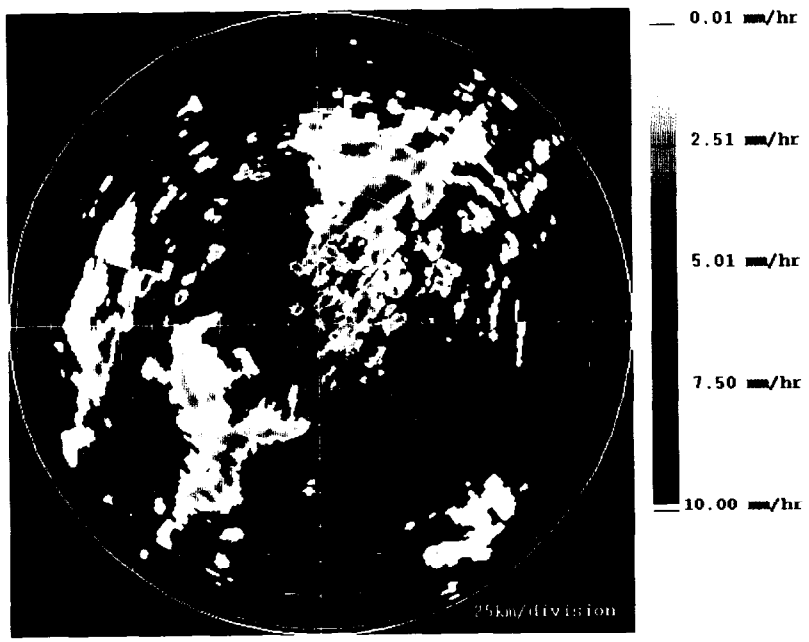

Fig. 1. Winter type storm (at 11:45 A.M.) monitored by National Severe Storms Laboratory, Norman, Oklahoma, on February 22, 1985. The field represents the average rainfall intensity (in millimeters per hour) over 5 min interval. The vertical represents the north-south direction and the radial marks are 25 km apart.

115 estimates for a range of 230 km (i.e., data at every 2 km by 1 degree). Rainfall intensities for the winter storm are available only at temporal integration scales of 5 min intervals. Intensities at the 1-hour integration scale were obtained by averaging 12 consecutive nonoverlapping 5 min scans. Intensity values for each radar scan over the 360 azimuths will henceforth be referred to as a "frame." The precipitation processing system, used to correlate reflectivity and rainfall intensity, taking into account the raingage observations, and adjustment for ground clutter, etc., is described by *O'Bannon and Ahnert* [1986]. For the purpose of our analysis the data were converted to a rectangular grid of size 512 × 512 by bilinear interpolation on the polar grid. For future reference we will use the following mnemonics for the above data sets: S1, squall line data at 1 hour integration time; S2, squall line data at 10 min integration time; W1, winter type storm data at 1 hour integration time; and W2, winter type storm data at 5 min integration time.

Frame 1 of the 10-min integrated intensities of squall line storm (data set S2) is displayed in Figure 13 of *Kumar and Foufoula-Georgiou* [this issue] and frame 1 of the 5-minute integrated intensities of winter type storm (data set W2) is displayed in Figure 1. Small-scale features of the above data sets were obtained using the multiscale decomposition approach using Haar wavelets as explained by *Kumar and Foufoula-Georgiou* [this issue].

Frame 1 of data sets S1, W1, and W2 and frame 3 of data set S2 were chosen for illustration of results, as they were characteristic of the behavior of the storm across several frames. Figure 2 shows empirical and theoretical cdfs for frame 1 of data set S1 after one level of decomposition of the original data set on a 512 × 512 grid; i.e., it shows cdf of the fluctuations on a grid of 256 × 256 for each of the components D_1, D_2, and D_3. Figure 3 shows the same plot for frame 1 of data set S2. The fit of the distribution at other levels of decomposition are similar and are not reported here. As is evident from Figures 2 and 3, the data set S2 shows a thicker tail and, consequently, lower value for α, as compared to data set S1, indicating that time integration has the effect of smoothing the violent behavior of the storm. Since data sets W1 and W2 correspond to a mild storm, the effect of time integration is not that dramatic in the estimates of α (see Figures 4 and 5) and the α values themselves are very close to 2, i.e., the distribution is almost Gaussian. Tables 1 and 2 give the estimates of α and scale parameter c for the first frame of each of the four data sets at six levels of decomposition. Table 1 shows some variation in the estimates of α with respect to scale which could be due to

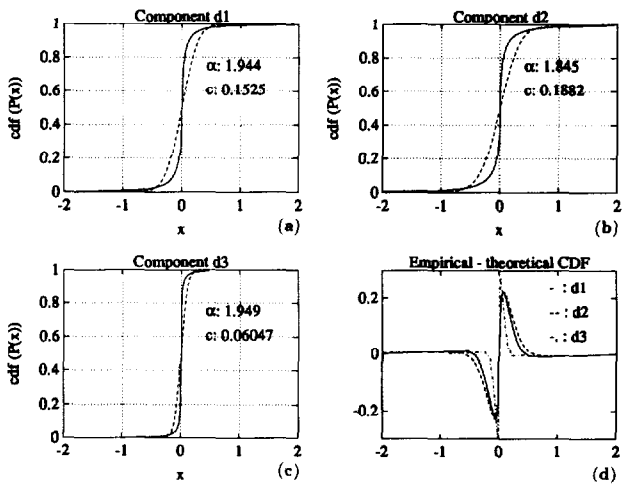

Fig. 2. Empirical (solid curves) and theoretical (dotted curves) cumulative distribution functions for the three components: (*a*) D_1, (*b*) D_2, and (*c*) D_3 of frame 1 of data set S1 (squall line storm at the 1-hour integration time) after one level of decomposition. Figure 2*d* shows the deviation between the empirical and theoretical cumulative distribution functions.

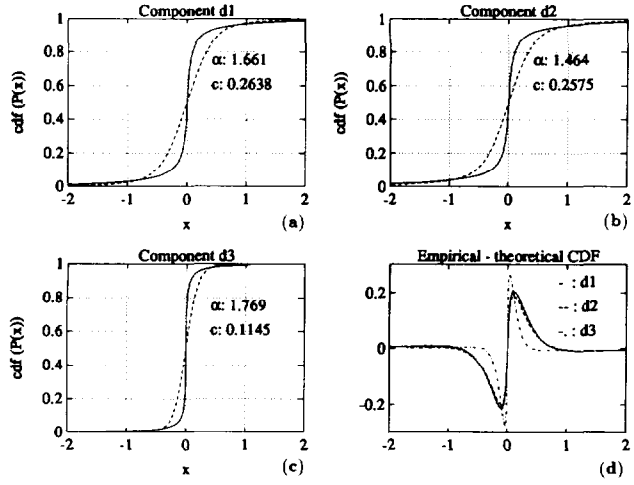

Fig. 3. Same as Figure 2 for frame 3 of data set S2 (squall line storm at the 10-min integration time).

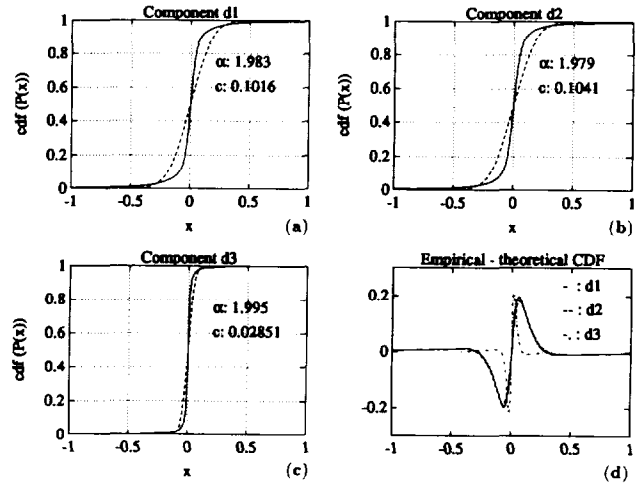

Fig. 5. Same as Figure 2 for frame 1 of data set W2 (winter type storm at the 5-min integration time).

sampling, or a limitation of the estimation technique, or the fluctuations may have different α at different scales. The exact cause for the variation is under investigation. For the current research, we will use the mean value of α (mean obtained over several scales) for each component as the representative value for that component.

In comparing the theoretical and empirical cdfs some remarks are in order. First, the empirical CDFs have been displayed using Weibull plotting position which is expected to be biased for stable distributions. We are not aware of any literature on the problem of choosing appropriate plotting positions for stable distributions. This issue needs further research. Second, no results of statistical testing, e.g., Kolmogorov-Smirnov or χ^2 tests, are reported for the comparison of empirical and theoretical distribution functions as these tests are appropriate for independent samples and their use on samples exhibiting long range dependence renders them weak and unreliable. Third, as is observed from Figures 2–5, the fitting is very good at the tails. This is desirable since as *Mandelbrot* [1963, p. 425] shows, the properties of samples of stable distribution are dominated by the tail behavior of the distribution. For example, if $X_n (1 \leq n \leq N)$ have a distribution with hyperbolic tails with the same α, i.e., $P(X_n > x) \sim C_n x^{-\alpha}$ (see property 3, section 2.3.1), then $P(\max\{X_n\} > x) \sim (\Sigma_n C_n) x^{-\alpha}$, i.e., the maximum is asymptotically hyperbolic with the same α; and $P(\Sigma_n X_n > x) \sim (\Sigma_n C_n) x^{-\alpha}$, i.e., the sum is asymptotically hyperbolic with the same α and behaves asymptotically like the largest of them. The consequence of the above properties is that any statistic of interest with regard to the random variables X_n will be dominated by a few large values and the contribution of the several small values is negligible, i.e., behavior of the tail is dominant. Notice that for the above invariance properties to hold, the distributions need not be exactly stable but that they have hyperbolic tails.

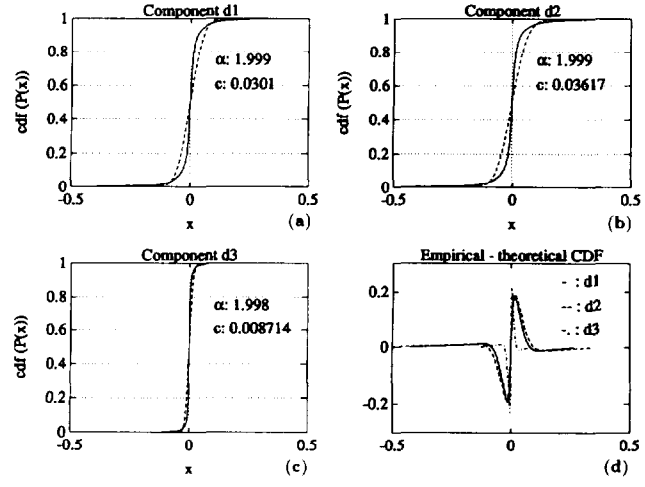

Fig. 4. Same as Figure 2 for frame 1 of data set W1 (winter type storm at the 1-hour integration time).

Recognizing that rainfall intensities are dependent, *Kedem et al.* [1990] fitted probability distributions using an estimation procedure based on minimizing the χ^2 statistic. Such an estimation procedure applied to our data resulted in a very good approximation of the body of the probability distribution function but very poor approximation at the tails, i.e., thicker tails (lower α). Such a fitting would be inappropriate given the sensitivity of the order statistics to the value of α. Estimation of parameters of stable distributions is an issue that has not been adequately addressed in the statistical/mathematical literature. Given the recent interest in long-range dependent processes and scaling models further research is needed in this area.

Figure 6 shows the log-log plot of the scale parameter c with respect to scale λ for frame 1 of data set S1, frame 3 of data set S2, and frame 1 of data sets W1 and W2 described in Tables 1 and 2. These frames were chosen because they are illustrative of the average behavior of the storms over several frames. As is clearly seen, data sets S1, S2, and W1 show log-log linearity of c with respect to λ indicating scaling up to five levels of decomposition, i.e., up to an averaging pixel size of 28.75 × 28.75 km. Data sets corresponding to the winter type storm show a different albeit interesting behavior. Although, the fluctuations at small temporal integration scales (5 min) do not show any significant scaling, they exhibit scaling behavior at the larger temporal integration scale of 1 hour, and this result is consistent across frames. Significant variations were observed in the estimates of H between the data sets S1 and S2 where scaling was

TABLE 1. Estimates of α and c for the Squall Line Storm at Various Levels of Decomposition

	Frame 1 of S1 (11:40 A.M. to 12:40 P.M.)					Frame 3 of S2 (12:11 A.M. to 12:21 P.M.)				
Grid	α	c	$\bar{\alpha}$	H	r	α	c	$\bar{\alpha}$	H	r
				Component D_1						
256 × 256	1.944	0.152				1.661	0.264			
128 × 128	1.885	0.213				1.587	0.360			
64 × 64	1.904	0.262				1.573	0.468			
32 × 32	1.939	9.289				1.673	0.543			
16 × 16	1.942	0.390	1.923	0.315	0.985	1.775	0.588	1.654	0.291	0.972
8 × 8	1.986	0.449				1.967	0.609			
4 × 4	2.000	0.512				2.000	0.522			
				Component D_2						
256 × 256	1.845	0.188				1.463	0.257			
128 × 128	1.722	0.240				1.354	0.341			
64 × 64	1.491	0.259				1.269	0.404			
32 × 32	1.509	0.331				1.305	0.540			
16 × 16	1.635	0.467	1.640	0.309	0.980	1.461	0.722	1.371	0.364	0.997
8 × 8	1.929	0.612				1.897	0.643			
4 × 4	1.979	0.958				1.924	1.090			
				Component D_3						
256 × 256	1.949	0.060				1.768	0.114			
128 × 128	1.952	0.116				1.720	0.212			
64 × 64	1.883	0.181				1.466	0.249			
32 × 32	1.770	0.220				1.642	0.410			
16 × 16	1.864	0.350	1.884	0.549	0.980	1.785	0.580	1.677	0.564	0.988
8 × 8	1.949	0.339				1.968	0.477			
4 × 4	2.000	0.404				2.000	0.405			

Also given are the mean $\bar{\alpha}$ and H estimated using the first five levels of decomposition. The correlation coefficient r for the estimation of H is also indicated.

observed at both large and small temporal integration scales. This behavior was consistently observed for other frames in each of the data sets. These results have far reaching implications since they indicate significant variation in the type of scaling at different temporal integration scales and from storm to storm.

Table 3 gives the estimates of $\bar{\alpha}_i$ and H for each component D_1, D_2, and D_3 for several frames in each of the data

TABLE 2. Estimates of α and c for the Winter Type Storm at Various Levels of Decomposition

	Frame 1 of W1 (11:45 A.M. to 12:47 P.M.)					Frame 1 of W2 (11:45 A.M. to 11:50 A.M.)				
Grid	α	c	$\bar{\alpha}$	H	r	α	c	$\bar{\alpha}$	H	r
				Component D_1						
256 × 256	1.998	0.030				1.983	0.101			
128 × 128	1.998	0.049				1.963	0.153			
64 × 64	1.996	0.071				1.943	0.195			
32 × 32	1.995	0.090				1.978	0.204			
16 × 16	1.998	0.098	1.997	0.0488	0.966	1.976	0.160	1.968	0.171	0.681
8 × 8	1.999	0.120				1.998	0.135			
4 × 4	2.000	0.144				2.000	0.135			
				Component D_2						
256 × 256	1.999	0.036				1.978	0.104			
128 × 128	1.998	0.060				1.947	0.154			
64 × 64	1.996	0.089				1.932	0.209			
32 × 32	1.994	0.121				1.965	0.221			
16 × 16	1.996	0.133	1.996	0.477	0.973	1.997	0.147	1.964	0.153	0.552
8 × 8	1.996	0.161				1.996	0.153			
4 × 4	2.000	0.109				2.000	0.159			
				Component D_3						
256 × 256	1.998	0.008				1.995	0.029			
128 × 128	2.000	0.018				1.993	0.059			
64 × 64	1.998	0.039				1.989	0.098			
32 × 32	1.996	0.068				1.979	0.154			
16 × 16	1.995	0.097	1.997	0.880	0.991	1.984	0.138	1.988	0.594	0.938
8 × 8	1.995	0.102				1.992	0.127			
4 × 4	2.000	0.072				2.000	0.064			

Also given are the mean $\bar{\alpha}$ and H estimated using the first five levels of decomposition. The correlation coefficient r for the estimation of H is also indicated.

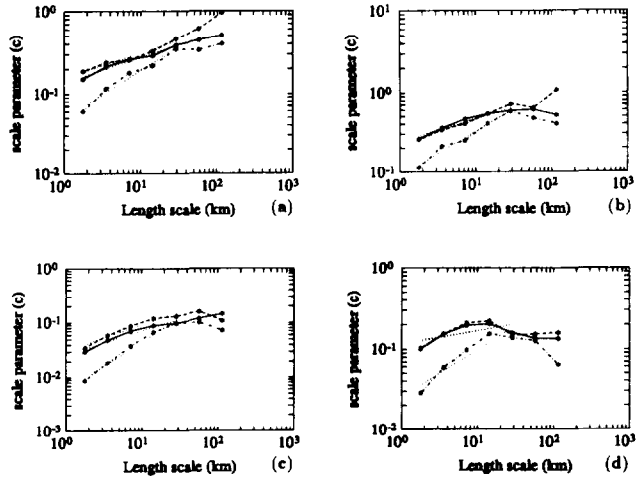

Fig. 6. Log-log plot of scale parameter with respect to scale for frame 1 of (*a*) data set S1, (*b*) frame 3 of data set S2, and frame 1 of (*c*) data set W1 and (*d*) data set W2. The solid line is for component D_1, dotted line is for D_2, and dotted-dashed line is for D_3. The regression lines obtained using five levels of decomposition are also indicated. The slope H and the correlation coefficient r for the regression lines are given in Tables 1 and 2.

sets S1 and S2. Each estimate is obtained by considering five levels of decomposition. Figure 7 shows the plot of these values which describe the evolutionary behavior of the storm. As can be seen, $\bar{\alpha}_i$ shows significant variation at small temporal integration scales and is almost constant for large integration scales (Figure 7*b*). The values of $\bar{\alpha}_i$ increase (Figure 7*b*) as the storm goes through the dissipative stages (recall that the squall line data were available beginning only at the mature stage of the core of the storm), and this is interpreted as the consequence of the decaying of the core of the squall line which reduces the variability of the rainfall intensities. A similar pattern, but with lesser variation, is observed at larger temporal integration scales (Figure 7*a*).

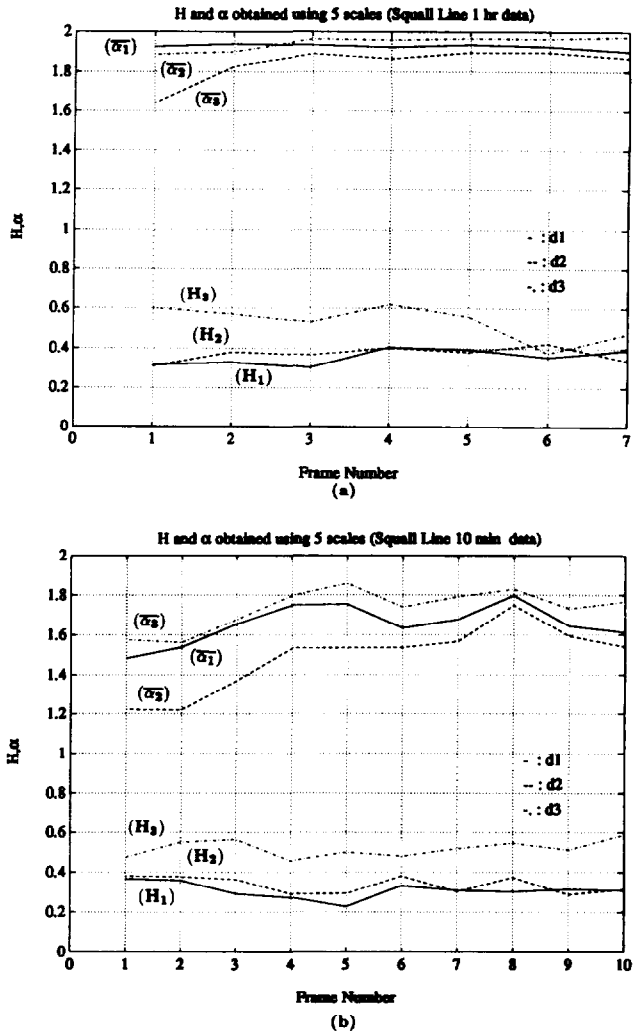

Fig. 7. Time evolution of $\bar{\alpha}_i$ and H_i: data set S1 (*a*) and data set S2 (*b*) (see Table 3 for exact values).

TABLE 3. Estimates of $\bar{\alpha}_i$ and H for Each Component D_1, D_2, and D_3 Obtained Using Five Levels of Decomposition, Across Several Frames for the Squall Line Data

		D_1		D_2		D_3	
Frame	Time	$\bar{\alpha}_1$	H_1	$\bar{\alpha}_2$	H_2	$\bar{\alpha}_3$	H_3
		Data Set S1					
1	11:40 A.M. to 12:40 P.M.	1.923	0.315	1.640	0.309	1.884	0.599
2	12:38 P.M. to 1:38 P.M.	1.935	0.328	1.826	0.380	1.897	0.570
3	2:38 P.M. to 3:38 P.M.	1.931	0.303	1.887	0.367	1.960	0.530
4	3:37 P.M. to 4:37 P.M.	1.919	0.406	1.862	0.402	1.955	0.618
5	4:35 P.M. to 5:35 P.M.	1.932	0.394	1.893	0.381	1.963	0.558
6	5:33 P.M. to 6:33 P.M.	1.922	0.355	1.893	0.424	1.961	0.376
7	6:31 P.M. to 7:31 P.M.	1.897	0.392	1.865	0.338	1.971	0.474
		Data Set S2					
1	11:52 A.M. to 12:02 P.M.	1.483	0.366	1.222	0.381	1.575	0.475
2	12:02 P.M. to 12:11 P.M.	1.538	0.359	1.219	0.377	1.562	0.550
3	12:11 P.M. to 12:21 P.M.	1.654	0.291	1.371	0.364	1.677	0.564
4	12:21 P.M. to 12:31 P.M.	1.747	0.272	1.533	0.291	1.796	0.456
5	12:31 P.M. to 12:40 P.M.	1.753	0.227	1.534	0.292	1.858	0.500
6	12:40 P.M. to 12:50 P.M.	1.632	0.332	1.536	0.381	1.738	0.480
7	12:50 P.M. to 1:00 P.M.	1.676	0.308	1.566	0.303	1.791	0.518
8	1:00 P.M. to 1:10 P.M.	1.797	0.302	1.748	0.375	1.830	0.546
9	1:10 P.M. to 1:19 P.M.	1.643	0.315	1.593	0.288	1.731	0.512
10	1:19 P.M. to 1:29 P.M.	1.612	0.309	1.540	0.315	1.766	0.588

However, during the dissipative phase the $\bar{\alpha}_i$ values remain almost constant indicating no significant variation in the nature of the (tail of the) distribution functions. A similar analysis for the winter type storm indicated that the rainfall fluctuations at the 5-min integration scale (data set W2) do not exhibit significant scaling. For an integration interval of 1 hour scaling was observed, but since the storm lasted only 3.5 hours the nature of the temporal variation of these parameters could not be established.

6. Conclusions

The multicomponent decomposition methodology presented in these companion papers provides a new approach to space-time rainfall analysis for segregating large- and small-scale features, and identifying and estimating the nature of self-similarity in the small-scale features (fluctuations). This decomposition approach makes no a priori assumption about the structure of the rainfall fields. If self-similarity is found to be present in the fluctuations, the maximum scale over which it holds is used to define the scale below which physical or other nonscaling stochastic descriptions should be sought. The idea behind this approach is that the large-scale features represent the morphological organization or large-scale forcing specific to the particular rain producing mechanisms and are scale dependent, whereas when this effect is subtracted the resulting deviations might exhibit scale invariant characteristics.

The analysis of two storms has indicated that rainfall fluctuations, when appropriately decomposed to account for anisotropy exhibit self-similar characteristics whose nature persists over the evolution of the storm. The range over which self-similarity holds and the type of self-similarity depend on the storm type and for a particular storm on the temporal integration scale at which the description of the rainfall process is sought. For example, the squall line rainfall fluctuations exhibited self-similar characteristics over all the three directional components (D_1, D_2, and D_3) up to a scale of 25–30 km, and this long-range dependence was stronger at the 1-hour integration scale as compared to the 10-min integration scale. For the winter type storm, the rainfall fluctuations derived from the 5-min integrated data did not show any self-similarity, although the 1-hour integrated data exhibited self-similarity. Unfortunately, its time evolution was hard to characterize due to the short duration of this storm. It is interesting to note that these results were further corroborated with a different method of analysis based on probability-weighted moments [see *Kumar et al.*, 1992].

Taylor's hypothesis has been observed to hold for rainfall intensities for time period up to 40 min [*Zawadzki*, 1973]. *Gupta and Waymire* [1987] showed that for Taylor's hypothesis to be valid for some scales, scaling laws should hold for those scales, or vice versa. It is interesting to note that a time period of 40 min for a storm moving at the speed of 10–12.5 m/s correspond to a spatial scale of 24–30 km. The results reported in this research are remarkably consistent with the above observation.

It has been argued in previous studies [e.g., *Lovejoy and Schertzer*, 1987; *Gupta and Waymire*, 1990] that simple scaling models are just too simple to provide adequate description of rainfall intensities or rainfall fluctuations. Our analysis indicates that simple scaling models can indeed provide a good description of the rainfall fluctuation process if, however, this process is decomposed in a "clever" way to account for the anisotropic nature of the storms. Note that if each one of these three components D_1, D_2, and D_3 is described by a simple scaling model, it does not mean that the composite process of rainfall fluctuations is also simple scaling. We propose to call such a process "multicomponent scaling."

Unlike other current approaches, our method provides the ability to (1) analyze the data and let them tell us what structure is present rather than imposing a structure a priori, (2) account for anisotropy and inhomogeneities, and (3) characterize the evolutionary structure of the storm. If self-similarity is found to be present it is described by nine parameters (three in each direction) for which we have provided estimation procedures which do not suffer from the two main drawbacks of current moment analysis methods: unreliability of higher-order moments and estimation of moments where, in fact, theoretical moments of the hypothesized distributions do not exist.

In this paper we have presented analysis of rainfall fields based on the proposed approach. Modeling and simulation of rainfall fields have not been discussed but are feasible further extensions to be pursued. An interesting application of a modeling/simulation approach based on the proposed methodology will be on subgrid scale parameterization and coupling physical large-scale models with stochastic small-scale descriptions. The absence of proper physical and dynamical understanding of the precipitation process at a range of scales of interest has lead hydrologists to resort to completely stochastic models for diverse applications. The point process models of *Waymire et al.* [1984], multifractal models of *Lovejoy and Schertzer* [1987], and more recent random cascade models of *Gupta and Waymire* [1993] have been geared toward this direction. However, over the last decade, due to an increased understanding of atmospheric phenomena and availability of more powerful computers, there has been a revolutionary improvement in our ability to physically model regional and mesoscale atmospheric phenomena. Clearly, models based on physical and dynamical considerations are far superior to those based on purely stochastic considerations. It is believed that coupling physical and stochastic approaches provides an interesting and promising avenue for significant further improvements in rainfall modeling research. The methodologies presented in this paper should be explored toward this direction since the obtained results indicate that at least for some types of storms, scaling characteristics in rainfall fluctuations seem to hold up to a scale of 30 × 30 km, which is the resolution of most mesoscale weather models (see, for example, *Pielke* [1984]). Therefore multicomponent scaling models of the type proposed herein, which are efficient and consistent across scales, could be used for subgrid statistical parameterization of rainfall in mesoscale weather prediction models.

The line of research presented here opens several questions that deserve further study. For example, we have seen that the small-scale statistical parameterization varies from storm to storm, and we anticipate that it relates to the large-scale dynamics, for example, the storm type and the environmental conditions of the rain producing mechanism. Indeed, it is true that there is a feedback mechanism between large and small scales. This is also evident from the results reported in paper 1 [*Kumar and Foufoula-Georgiou*, this issue] where it was identified that large fluctuations were

observed in regions of large mean values. As a first level of approximation we ignored this effect and considered the component fields to be homogeneous for the purpose of statistical characterization. The results, even with this approximation, are very satisfactory. Further advances can be made by studying the small-scale features conditioned on the large-scale features to account for the observed inhomogeneities. It is remarked that the small-scale statistical characterization we provide is linear in the sense that it is based on a linear simple scaling model for each of the three components. It can be argued that such a linear modeling framework may not be adequate given the nonlinear nature of the processes governing the formation of precipitation. However, as in many other processes, linear analysis often offers good approximations to nonlinear processes and due to its simplicity should not be discarded as inappropriate but explored to its full extent, as done here. In fact, the results from the data sets analyzed indicated that the linear approximation was satisfactory for the description of rainfall fluctuations for these two storms. Another issue that needs further study is the effect of the choice of wavelets and the choice of separable multiresolution framework on the obtained results. One could explore other multiresolution frameworks or decompositions with more directional selectivity depending on the process at hand.

Appendix: Fractional Levy Motion

Continuous self-similar processes with increments having stable marginal distribution and long range dependence are called fractional Levy motions (fLm). Here we give a particular construction of fLm which is based on the idea in the work by *Taqqu* [1987, equation 14] and specializes to fractional Brownian motion for $\alpha = 2$. The objective is to develop a process whose increments are stationary, have stable distribution, and show long-range dependence similar to fBm.

Define

$$R_{X_u,X_v}(u, v) = \frac{\nu}{2}\left[|u|^{2H} + |v|^{2H} - |u - v|^{2H}\right]$$

$$0 < H < 1,\ \nu \in \mathbf{R}^+ \qquad (38)$$

where $X_u = X(u)$ and $X_v = X(v)$ for a process $X(t)$. Let Ω be generated as $\Omega_{11} = R_{X_u,X_u}(u, u) = \nu|u|^{2H}$, $\Omega_{12} = \Omega_{21} = R_{X_u,X_v}(u, v)$, $\Omega_{22} = R_{X_v,X_v}(v, v) = \nu|v|^{2H}$; thus

$$\Omega = \frac{\nu}{2}\begin{bmatrix} 2|u|^{2H} & |u|^{2H} + |v|^{2H} - |u - v|^{2H} \\ |u|^{2H} + |v|^{2H} - |u - v|^{2H} & 2|v|^{2H} \end{bmatrix} \qquad (39)$$

Since $R_{X_u,X_v}(u, v)$ is a positive semidefinite symmetric kernel [see *Ossiander and Waymire*, 1989], Ω is a positive semidefinite symmetric matrix. Therefore the joint characteristic function of $X(u)$ and $X(v)$ is given by

$$\rho_{X_u,X_v}(\xi_u, \xi_v) = \exp\left\{ i(\mu_u\ \mu_v)\begin{pmatrix}\xi_u \\ \xi_v\end{pmatrix} - \frac{1}{2}\left((\xi_u\ \xi_v)\cdot\begin{pmatrix}\Omega_{11} & \Omega_{12} \\ \Omega_{21} & \Omega_{22}\end{pmatrix}\begin{pmatrix}\xi_u \\ \xi_v\end{pmatrix}\right)^{\alpha/2}\right\} \qquad (40)$$

The matrix Ω depicts the dependence structure of $X(t)$ and for $\alpha = 2$ it is the covariance matrix.

Consider the symmetric distributions located at the origin, i.e., $\mu = 0$ whose joint characteristic function is given as

$$\rho_X(\xi) = \exp\{-\tfrac{1}{2}(\xi \cdot \Omega\xi)^{\alpha/2}\} \qquad (41)$$

The marginal characteristic function of $X(u)$ is given by

$$\rho_{X_u}(\xi_u) = \rho_{X_u,X_v}(\xi_u, 0) = \exp\{-\tfrac{1}{2}(\Omega_{11}\xi_u^2)^{\alpha/2}\}$$

$$= \exp\{-\tfrac{1}{2}(\Omega_{11}^{1/2}\xi_u)^{\alpha}\} \qquad (42)$$

Under the condition of stationary increments and $X(0) = 0$, this also gives the characteristic function of the distribution of the increments with the scale parameter c given by (after substituting for Ω_{11})

$$c = \left(\frac{1}{2}\right)^{1/\alpha}\sqrt{\nu}\,|u|^H \qquad (43)$$

or, equivalently, substituting λ for u

$$\log c = H \log \lambda + \log \kappa \qquad (44)$$

for some constant $\kappa \in R^+$. We can use this to study the behavior of the scale parameter c with change in scale λ and also estimate H.

Notice that for $H = 1/\alpha$ the above expressions reduces to that of stable Levy motion. Long range positive dependence of increments of fLm occurs for $1/\alpha < H < 1$, $1 < \alpha \le 2$ [see *Taqqu*, 1987]. It is easy to verify that

$$\rho_{X_{\lambda u},X_{\lambda v}}(\xi_u, \xi_v) = \rho_{X_u,X_v}(\lambda^H\xi_u, \lambda^H\xi_v) \qquad (45)$$

indicating that $X(t)$ is self-similar with parameter H (see equation (11)).

Acknowledgments. This research was supported by National Science Foundation grants BSC-8957469 and EAR-9117866 and by NASA grant NAG 5-2108 and a Graduate Student Fellowship for Global Change Research. We also thank the Minnesota Supercomputer Institute for providing us with supercomputer resources and Tim O'Bannon of NEXRAD Operational Support Facility, Norman, Oklahoma, for providing us with the rainfall data.

References

Arad, R. W., Parameter estimation for symmetric stable distribution, *Int. Econ. Rev.*, *21*(1), 209–220, 1980.

Daubechies, I., *Ten Lectures on Wavelets*, Society for Industrial and Applied Mathematics, Philadelphia, Pa., 1992.

Dobrushin, R. L., Automodel generalized randon fields and their renorm group, in *Multicomponent Random Systems*, Marcel Dekker, New York, 1978.

Feller, W., *An Introduction to Probability Theory and Its Applications*, vol. 2, John Wiley, New York, 1971.

Gawronski, W., On the bell shape of stable densities, *Ann. Probability*, *12*(1), 230–242, 1984.

Gupta, V., and E. Waymire, On Taylor's hypothesis and dissipation in rainfall, *J. Geophys. Res.*, *92*(D8), 9657–9660, 1987.

Gupta, V., and E. Waymire, Multiscaling properties of spatial rainfall and river flow distributions, *J. Geophys. Res.*, *95*(D3), 1999–2009, 1990.

Gupta, V., and E. Waymire, A statistical analysis of mesoscale rainfall as a random cascade, *J. Appl. Meteorol.*, *32*(2), 251–267, 1993.

Haan, C. T., *Statistical Methods in Hydrology*, 378 pp., Iowa State University Press, Ames, 1977.

Holt, D. R., and E. L. Crow, Tables and graphs of stable probability

density functions, *J. Res. Nat. Bur. Stand., Sect. B*, *77B*(3 and 4), 143–198, 1973.

Kedem, B., L. S. Chiu, and G. R. North, Estimation of mean rate: Application of satellite observations, *J. Geophys. Res.*, *95*(D2), 1965–1972, 1990.

Kumar, P., and E. Foufoula-Georgiou, Multicomponent decomposition of spatial rainfall fields, 1, Segregation of large- and small-scale features using wavelet transforms, *Water Resour. Res.*, this issue.

Kumar, P., P. Guttorp, and E. Foufoula-Georgiou, A probability weighted moment test to assess scaling in rainfall, *Rep. UMSI 92/278*, Supercomputer Inst., Univ. of Minn., Minneapolis, Dec. 1992.

Lamperti, J., Semi-stable stochastic processes, *Trans. Am. Math. Soc.*, *104*, 62–78, 1962.

Lovejoy, S., and D. Schertzer, Physical modeling and analysis of rain and clouds by anisotropic scaling multiplicative processes, *J. Geophys. Res.*, *92*(D8), 9693–9714, 1987.

Mandelbrot, B., New methods in statistical economics, *J. Political Econ.*, *71*(5), 421–440, 1963.

O'Bannon, T., and P. Ahnert, A study of the NEXRAD precipitation processing system on a winter-type Oklahoma rainstorm, paper presented at 23rd Conference on Radar Meteorology and the Conference on Cloud Physics, Am. Meteorol. Soc., Snowmass, Colo., Sept. 22–26, 1986.

Ossiander, M., and E. Waymire, Certain positive-definite kernels, *Proc. Am. Math. Soc.*, *107*(2), 487–492, 1989.

Paulauskas, V. J., Some remarks on multivariate stable distributions, *J. Multivar. Anal.*, *6*, 356–368, 1976.

Pielke, R. A., *Mesoscale Meteorological Modeling*, Academic, San Diego, Calif., 1984.

Press, S. J., Multivariate stable distributions, *J. Multivar. Anal.*, *2*, 444–462, 1972.

Press, S. J., *Applied Multivariate Analysis*, Robert E. Krieger, Huntington, N. Y., 1982.

Stuart, A., and J. K. Ord, *Kendall's Advanced Theory of Statistics*, Vol. 1, Oxford University Press, New York, 1987.

Taqqu, M., Random processes with long-range dependence and high variability, *J. Geophys. Res.*, *92*(D8), 9683–9686, 1987.

Waymire, E., V. K. Gupta, and I. Rodriguez-Iturbe, A spectral theory of rainfall intensity at the meso-β scale, *Water Resour. Res.*, *20*(10), 1453–1465, 1984.

Zawadzki, I. I., Statistical properties of precipitation patterns, *J. Appl. Meteorol.*, *12*, 459–472, 1973.

Zolotarev, V. M., *One Dimensional Stable Distributions, Transl. 65*, 284 pp., American Mathematical Society, Providence, R. I., 1986.

E. Foufoula-Georgiou, St. Anthony Falls Hydraulic Laboratory, Department of Civil and Mineral Engineering, University of Minnesota, Mississippi River and Third Avenue, Southeast, Minneapolis, MN 55414.

P. Kumar, USRA, Hydrologic Sciences Branch, Laboratory for Hydrospheric Processes, Code 974, Building 22, NASA Goddard Space Flight Center, Greenbelt, MD 20771.

(Received July 23, 1992;
revised February 11, 1993;
accepted March 4, 1993.)